Mutations in *EXTL3* Cause Neuro-immuno-skeletal Dysplasia Syndrome

Machteld M. Oud,[1,26,*] Paul Tuijnenburg,[2,3,26] Maja Hempel,[4,26] Naomi van Vlies,[5] Zemin Ren,[6] Sacha Ferdinandusse,[5] Machiel H. Jansen,[2,3] René Santer,[7] Jessika Johannsen,[7] Chiara Bacchelli,[8] Marielle Alders,[9] Rui Li,[10,11] Rosalind Davies,[8] Lucie Dupuis,[12] Catherine M. Cale,[13] Ronald J.A. Wanders,[5] Steven T. Pals,[6] Louise Ocaka,[8] Chela James,[8] Ingo Müller,[14] Kai Lehmberg,[14] Tim Strom,[15,16] Hartmut Engels,[17] Hywel J. Williams,[8] Phil Beales,[8] Ronald Roepman,[1] Patricia Dias,[18] Han G. Brunner,[1] Jan-Maarten Cobben,[19,20] Christine Hall,[21] Taila Hartley,[22] Polona Le Quesne Stabej,[8] Roberto Mendoza-Londono,[12] E. Graham Davies,[8,13] Sérgio B. de Sousa,[8,23,24] Davor Lessel,[4,27] Heleen H. Arts,[1,25,27] and Taco W. Kuijpers[2,27,*]

EXTL3 regulates the biosynthesis of heparan sulfate (HS), important for both skeletal development and hematopoiesis, through the formation of HS proteoglycans (HSPGs). By whole-exome sequencing, we identified homozygous missense mutations c.1382C>T, c.1537C>T, c.1970A>G, and c.2008T>G in *EXTL3* in nine affected individuals from five unrelated families. Notably, we found the identical homozygous missense mutation c.1382C>T (p.Pro461Leu) in four affected individuals from two unrelated families. Affected individuals presented with variable skeletal abnormalities and neurodevelopmental defects. Severe combined immunodeficiency (SCID) with a complete absence of T cells was observed in three families. EXTL3 was most abundant in hematopoietic stem cells and early progenitor T cells, which is in line with a SCID phenotype at the level of early T cell development in the thymus. To provide further support for the hypothesis that mutations in *EXTL3* cause a neuro-immuno-skeletal dysplasia syndrome, and to gain insight into the pathogenesis of the disorder, we analyzed the localization of EXTL3 in fibroblasts derived from affected individuals and determined glycosaminoglycan concentrations in these cells as well as in urine and blood. We observed abnormal glycosaminoglycan concentrations and increased concentrations of the non-sulfated chondroitin disaccharide D0a0 and the disaccharide D0a4 in serum and urine of all analyzed affected individuals. In summary, we show that biallelic mutations in *EXTL3* disturb glycosaminoglycan synthesis and thus lead to a recognizable syndrome characterized by variable expression of skeletal, neurological, and immunological abnormalities.

Introduction

A number of complex immunodeficiency syndromes additionally include skeletal dysplasia as part of their variable phenotype. For example, Schimke immuno-osseous dysplasia (SIOD [MIM: 242900]) and cartilage-hair hypoplasia (CHH [MIM: 250250]) are (spondylo-epiphyseal-) metaphyseal dysplasias that can also result in disproportionate short stature.[1–3] Besides featuring skeletal dysplasia, CHH is further characterized by T cell immunodeficiency, brittle hair, ligamentous laxity, hypoplastic anemia, and sometimes neuronal dysplasia of the intestine, leading to Hirschsprung disease.[4] SIOD is commonly associated with skeletal dysplasia, nephropathy, and T cell immunodeficiency (GeneReviews, see Web Resources). Notably, both CHH and SIOD are recessive disorders caused by mutations in *RMRP* (MIM: 157660) and *SMARCAL1* (MIM: 606622), respectively,[4,5] and affected individuals display both broad

[1]Department of Human Genetics, Radboud Institute for Molecular Life Sciences, Radboud University Medical Centre, PO Box 9101, 6500 HB Nijmegen, the Netherlands; [2]Department of Experimental Immunology, Academic Medical Centre, PO Box 22660, 1100 DD Amsterdam, the Netherlands; [3]Department of Pediatric Hematology, Immunology, and Infectious disease, Academic Medical Centre, PO Box 22660, 1100 DD Amsterdam, the Netherlands; [4]Institute of Human Genetics, University Medical Center Hamburg-Eppendorf, 20246 Hamburg, Germany; [5]Laboratory Genetic Metabolic Diseases, Academic Medical Centre, PO Box 22660, 1100 DD Amsterdam, the Netherlands; [6]Department of Pathology, Academic Medical Center, University of Amsterdam, PO Box 22660, 1100 DD Amsterdam, the Netherlands; [7]Department of Pediatrics, University Medical Center Hamburg-Eppendorf, 20246 Hamburg, Germany; [8]COSgene, Great Ormond Street Institute of Child Health, University College London, WC1N 1EH London, UK; [9]Department of Clinical Genetics, Academic Medical Center, University of Amsterdam, PO Box 22660, 1100 DD Amsterdam, the Netherlands; [10]Department of Human Genetics, McGill University, Montreal, QC H3A 1B1, Canada; [11]McGill University and Génome Québec Innovation Centre, Montreal, QC H3A 0G1, Canada; [12]Division of Clinical and Metabolic Genetics, Department of Paediatrics, The Hospital for Sick Children and University of Toronto, Toronto, ON M5G 1X8, Canada; [13]Department of Immunology, Great Ormond Street Hospital, WC1N 3JH London, UK; [14]Division of Pediatric Stem Cell Transplantation and Immunology, University Medical Center Hamburg-Eppendorf, 20246 Hamburg, Germany; [15]Institute of Human Genetics, Helmholtz Zentrum München, 85764 Neuherberg, Germany; [16]Institute of Human Genetics, Technische Universität München, 81675 München, Germany; [17]Institute of Human Genetics, University of Bonn, 53127 Bonn, Germany; [18]Serviço de Genética, Departamento de Pediatria, Hospital de Santa Maria, Centro Hospitalar Lisboa Norte, Centro Académico de Medicina de Lisboa, 1640-035 Lisboa, Portugal; [19]Department of Pediatrics, Academic Medical Center University Hospital, PO Box 22660, 1100 DD Amsterdam, the Netherlands; [20]Department of Clinical Genetics, St. George's University Hospital, SW19 0ER London, UK; [21]Emerita, Department of Radiology, Great Ormond Street Hospital, WC1N 3JH London, UK; [22]Children's Hospital of Eastern Ontario Research Institute, Ottawa, ON K1H 8 L1, Canada; [23]Medical Genetics Unit, Hospital Pediátrico, Centro Hospitalar e Universitário de Coimbra, 3000-602 Coimbra, Portugal; [24]Faculty of Health Sciences, University of Beira Interior, 6200-506 Covilhã, Portugal; [25]Department of Pathology and Molecular Medicine, McMaster University Medical Centre, Hamilton, ON L8S 4J9, Canada
[26]These authors contributed equally to this work
[27]These authors contributed equally to this work
*Correspondence: machteld.oud@radboudumc.nl (M.M.O.), t.w.kuijpers@amc.uva.nl (T.W.K.)
http://dx.doi.org/10.1016/j.ajhg.2017.01.013.
© 2017 American Society of Human Genetics.

interfamilial and intrafamilial variability of the immunological abnormalities (GeneReviews and Ridanpää et al.[4]).

Here, we report on a neuro-immuno-skeletal disorder caused by pathogenic mutations in *EXTL3* (exostosin-like glycosyltransferase 3 [MIM: 605744]), a gene not previously associated with human disease. EXTL3 is a member of the exostosin (EXT) family of glycosyltransferases, comprising EXT1, EXT2, EXTL1, and EXTL2. These enzymes regulate glycosylation, a process by which glycans are attached to both proteins and lipids in the endoplasmic reticulum or Golgi complex. EXTL3 and its family members are known to be involved in the biosynthesis of the glycosaminoglycan (GAG) heparan sulfate (HS) in a variety of species.[6–11] EXT family members exert an effect on many physiological activities by the covalent binding of HS chains to proteoglycans, forming HS proteoglycans (HSPGs). HSPGs are a major component of the extracellular matrix (ECM) in all organs in the human body and are involved in numerous physiological processes.[12] Notably, there are three subfamilies of HSPGs: membrane-spanning proteoglycans, glycophosphatidylinositol-anchored proteoglycans, and secreted ECM proteoglycans,[12] all of which have been implicated in skeletogenesis and hematopoiesis.[13,14]

EXTL3 is a *N*-acetylglucosaminyltransferase (GlcNac transferase) that exhibits GlcNac-TI activity by catalyzing GlcNac binding to a GAG linkage region, thereby initiating the biosynthesis of HS chains. EXTL2 shares GlcNac-TI activity with EXTL3 but initiates HS chains on different core proteins than EXTL3 by discriminating the amino acid sequences.[9] EXTL1 is involved in the elongation of HS chains by exhibiting GlcNAcT-II activity,[9] whereas the EXT family members EXT1 and EXT2 form a heterooligomeric complex with GlcNAc and GlcA transferase activity essential for the polymerization of HS. The crucial role of EXTL3 in general organogenesis is exemplified by embryonic lethality of mice homozygous for a null mutation.[11] Regarding human disorders, *EXT1* (MIM: 608177) and *EXT2* (MIM: 608210) are associated with autosomal-dominant hereditary multiple exostoses (MIM: 133700 and 133701, respectively).[15] In addition, autosomal-recessive mutations in *EXT2* lead to seizures, scoliosis, and macrocephaly syndrome (MIM: 616682).[16] *EXTL3* mutations have not yet been connected to any disease. In this report, we describe nine individuals from five unrelated families affected by an autosomal-recessive neuro-immuno-skeletal dysplasia syndrome caused by biallelic missense mutations in *EXTL3*.

Material and Methods

Collection of Samples and Informed Consent

For all five families, DNA samples were extracted from blood according to standard laboratory practice and used for whole-exome sequencing (WES). Fibroblast lines obtained from skin biopsy material of the affected individuals (A:II-1, B:II-1, B:II-2, C:II-1, D:III-1, D:IV-1, and E:II-1) and three in-house control fibroblast lines were used for GAG analysis and immunocytochemistry. Heparinized peripheral-blood samples and urine were collected from healthy age-matched control individuals and from affected individuals during routine diagnostic procedures. Urine collected from affected individuals A:II-1, B:II-1, and B:II-2 and serum collected from the blood of these individuals and parents B:I-1 and B:I-2 were used for GAG analysis. After identification of the *EXTL3* mutations in family A, other genetic laboratories were contacted via GeneMatcher and Matchmaker Exchange; this linked our EXTL3 submission to PhenomeCentral, resulting in the ascertainment of families B–E.[17–19] All participants in this study gave written informed consent, and all human material was collected after approval by the local ethic committees (NL40332.078.12 for family A, PV3802 for family B, 1000029424 for family C, 09CM32 for family D, and 06/Q0508/16 for family E).

WES

Genomic DNA from the unaffected parents and affected individuals II-1 (family A), II-1 and II-2 (family B), II-1 and her unaffected parents (family C), III-1, III-2, and IV-1 (family D), and II-1, II-2, and their unaffected parents (family E) were used for WES. WES experiments were performed in different centers with slightly different procedures that have essentially been described before (family A,[20–23] family B,[24] family C,[25,26] and families D and E[27]). In brief, exome enrichment was performed with an Agilent SureSelect Human All Exon 50 Mb Kit (V4 for families A, D, and E; V5 for families B and C), and then sequencing was performed on a SOLiD 5500xl System (Thermo Fisher Scientific; family A), Illumina HiSeq 2500 (family B), or HiSeq 2000 (families C–E). Read mapping and single-base-pair variant and indel calling were performed with LifeScope Software v.2.1 (Life Technologies) for family A. For families B–E, reads were aligned to the human genome assembly (UCSC Genome Browser hg19) with the Burrows-Wheeler Aligner (v.0.5.87.5 for family B and v.0.7.7 for family C), and detection of genetic variation was performed with SAMtools (v.0.1.18), PINDEL (v.0.2.4t), and ExomeDepth (v.1.0.0). For family C, indel realignment and base recalibration were performed with Genome Analysis Toolkit (GATK) v.3.1.1. Duplicated reads were removed by Picard v.1.108, and genetic variation was detected with SAMtools (v.1.2) and BCFtools (v.1.2).[28] Variant calling for families D and E included GATK base quality score recalibration, indel realignment, and duplicate removal. SNP and indel discovery and genotyping were performed with standard hard filtering parameters or variant quality score. The variant annotation and interpretation analyses were generated by Ingenuity Variant Analysis software (v.3.1.20140902, QIAGEN).

Copy-number variation (CNV) detection was performed on WES data of each affected individual. For family A, the CoNIFER computational pipeline[29] was used as described previously.[30] For family C, FishingCNV software[31] was used to call CNVs and compare the read depth of these CNVs against the distribution of reads in more than 50 control samples without related genetic disorders (all samples were sequenced and aligned according to the same protocol). In addition, the eXome-Hidden Markov Model (XHMM) algorithm was applied for the detection of rare CNVs.[32–34] A SNP array was then performed in affected individuals from family B as previously described.[35]

Bioinformatic Filtering

Variant annotation was performed with four independent in-house annotation pipelines. To prioritize variants in the sequencing data, we excluded variants that were non-genic, intronic (except for canonical splice sites), or synonymous. Further,

we excluded variants that were present in dbSNP 135 at a frequency > 1% or > 1% in the in-house variant database (2,096 in-house-analyzed exomes for family A and ~3,000 exomes for family C). For family C, variants with a minor allele frequency (MAF) > 5% in 1000 Genomes[36] (October 2014), the NHLBI Grand Opportunity (GO) Exome Sequencing Project (ESP) (v.0.0.30, November 3, 2014), or Exome Aggregation Consortium (ExAC) Browser (v.0.2, October 29, 2014) were excluded. Variants excluded in families D and E had a MAF > 1% in the NHLBI GO ESP and ExAC Browser. The NHLBI GO ESP contains data from more than 200,000 individuals. At the time of this study, the ExAC Browser included sequences of 60,706 unrelated individuals from different ethnic backgrounds. We used a quality filter to exclude variants with <5 reads or <20% variant reads. Candidate variants were validated by Sanger sequencing, and segregation analysis was conducted in all five families.

Immunophenotyping

Peripheral-blood mononuclear cells (PBMCs) were isolated by standard density gradient centrifugation techniques with Lymphoprep (Nycomed). For immunophenotyping, PBMCs were resuspended in phosphate buffered saline (PBS) containing 0.5% (w/v) bovine serum albumin (BSA) and 0.01% sodium azide and incubated with saturating concentrations of fluorescently labeled conjugated monoclonal antibodies. Cells were analyzed with a FACSCanto-II flow cytometer and FlowJo software. Samples from the affected individuals were analyzed simultaneously with PBMCs from healthy control individuals. The following conjugated monoclonal antibodies were used: CD4 PE-Cy7, CD8 PerCP-Cy5.5, CD20 PerCP-Cy5.5, CD27 APC, CD38 PE-Cy7, CD45 APC-H7, and IgD PE from BD Biosciences; CD3 Alexa 700 and CD19 Alexa 700 from eBioscience; CD27 FITC from Sanquin; CD45RA (2H4-RD1) PE from Beckman Coulter; IgM FITC and IgG FITC from Dako; and IgA FITC from Miltenyi Biotec.

In order to analyze the in vitro activation of T and B cells, we resuspended the PBMCs in PBS at a concentration of 5×10^6 to 10×10^6 cells/mL and labeled them with 0.5 μM carboxyfluorescein succinimidyl ester (CFSE) (Molecular Probes, Thermo Fisher Scientific) in PBS for 10 min at 37°C under constant agitation. Cells were washed and subsequently resuspended in Iscove's modified Dulbecco's medium (IMDM) supplemented with 10% fetal calf serum (FCS, BioWhittaker), antibiotics, and 3.57×10^{-4}% (v/v) β-mercaptoethanol (Merck). Labeled PBMCs containing a fixed number of B cells (2×10^4 per well) were cultured in 96-well flat-bottomed plates for 6 days at 37°C and stimulated with saturating amounts of anti-IgM mAb (clone MH15, Sanquin), anti-CD40 mAb (clone 14G7, Sanquin), and 20 ng/ml IL-21 (Invitrogen); 1 μg/mL CpG oligodeoxynucleotide 2006 (Invivogen) and 100 U/mL IL-2 (R&D Systems); or anti-CD3 (clone 1xE, Sanquin) and anti-CD28 (clone 15E8, Sanquin). We assessed the proliferation of B and T cells by measuring CFSE dilution by flow cytometry.

We assessed the secretion of IgG and IgM by mature B cells by analyzing supernatants for secreted IgM and IgG with an in-house ELISA assay using polyclonal rabbit anti-human IgM, IgG reagents, and a serum protein calibrator. All reagents were from Dako, as described previously.[37,38]

Validation of EXTL3 Antibody

We used a commercial antibody targeting EXTL3 (goat, AF2635, R&D Systems) to detect the level of EXTL3 in different cell lines and human tissue. In order to ensure the specificity of the antibody, we knocked out *EXTL3* in human embryonic kidney 293T (HEK293T) cells by using the CRISPR/Cas9 technique. Three different single guide RNAs (sgRNAs)—5′-CTTCTCTATAACGTCAGTAC-3′, 5′-GGGACTGGCTTTCGGCCTAT-3′, and 5′-AGAAGCTCGGGACCGCATCG-3′—were each inserted into a pLentiCRISPR v.2 vector (52961, Addgene) as described by Sanjana et al.[39] The pLentiCRISP v.2 construct containing the EXTL3 sgRNA or the empty vector was transfected into HEK293T cells with a Genius DNA Transfection Reagent (Westburg) according to the manufacturer's instructions. After transfection, we cultured the cells in standard cell-culture medium containing 2.5 μg/mL puromycin for 3 days to select only the transfected cells. Subsequently, we prepared and analyzed the cell lysates by western blotting to test the specificity of the EXTL3 antibody.

Analysis of EXTL3 in Lymphocytes and Thymus Tissue

We used western blotting to assess the level of EXTL3 in different lymphocyte cell lines. Protein lysates were made from diffuse large B cell lymphoma cell lines OCI-Ly1, OCI-Ly7, and U2932; myeloma cell lines ANBL6 and RPMI-8226; leukemia-derived T cell lines Jurkat, CCRF-CEM, and Molt4; T cell lymphoma cell line SupT1; Burkitt lymphoma cell line Namalwa; lymphoblast cell line Ramos; mobilized peripheral-blood $CD34^+$ progenitor cells; and $CD4^-CD8^-$, $CD4^+CD8^+$, $CD4^-CD8^+$, and $CD4^+CD8^-$ cells sorted from thymocytes. All cell lines were cultured in IMDM containing 10% fetal bovine serum and 100 units/mL penicillin. Protein lysates were separated by 10% sodium dodecyl sulfate polyacrylamide gel electrophoresis and subsequently immunoblotted according to a standard procedure. The immunoblots were incubated in PBS containing 5% milk and 0.2% tween with antibodies targeting human EXTL3 (goat, AF2635, R&D Systems) and β-actin (clone AC-15, mouse, A5441, Sigma Aldrich). Primary antibodies were detected by horseradish peroxidase (HRP)-conjugated secondary antibodies donkey-anti-goat (605-703-125, Rockland Immunochemicals) and rabbit-anti-mouse (P0161; Dako) and then detected by Amersham ECL Western Blotting Detection Reagent (GE Healthcare).

Paraffin-embedded thymus tissue for immunohistochemical investigations was obtained from a neonate who had died from asphyxia at birth and had a post-mortem examination unrelated to this study. To ensure optimal staining of EXTL3, we treated thymus tissue sections of 4 μm thickness with Tris ethylenediaminetetraacetic acid (EDTA, pH 9) for 20 min at 121°C for antigen retrieval. Sections were incubated overnight at 4°C with an antibody targeting human EXTL3 (goat, AF2635, R&D Systems). Subsequently, the tissues were washed with PBS and incubated with rabbit-anti-goat antibody (6160-01, Southern Biotech) for 30 min at room temperature. EXTL3 was detected by poly-HRP-anti-rabbit IgG (DPVR110HRP, Immunologic) and then by Ultra DAB (Immunologic).

Immunocytochemistry in Human Fibroblasts

The localization of EXTL3 was assessed in primary fibroblasts derived from A:II-1, B:II-1, and B:II-2 and compared with that in fibroblasts from two healthy control individuals. The fibroblasts were cultured in Dulbecco's modified Eagle's medium with 20% FCS on sterile coverslips for 72 hr and subsequently immunostained. For this purpose, cells were washed in PBS and fixed in 2% paraformaldehyde in PBS for 20 min. In order to enable antibody binding, we incubated cells in 10 mM sodium citrate buffer

Table 1. Overview of the Most Affected Organ Systems in All Affected Individuals

Abnormalities	A:II-1	B:II-1	B:II-2	C:II-1	D:III-1	D:III-2	D:IV-1	E:II-1	E:II-2
Neurological	NA	+++	+++	+	+[a]	–	–	NA	NA
Immunological	+++	+++	+++	–	–	–	–	++	++
Skeletal	+++	+	+	+++	+++	+++	+++	+++	+++

The number of plus signs indicates the severity of the abnormality. NA means not assessed because of early death (A:II-1 at 6 weeks, E:II-1 at 6 months, and E:II-2 at 10 months).
[a]Borderline normal cognition.

for 30 min at 60°C. Cells were then permeabilized in 1% Triton X-100 in PBS for 5 min and blocked for 30 min in 2% BSA in PBS. We used primary antibodies targeting EXTL3 at 1:100 dilution (goat, AF2635, R&D Systems) and the Golgi marker GM130 at 1:250 dilution (mouse, 610822, BD Biosciences). Primary antibodies were diluted in 2% BSA in PBS and incubated for 1 hr at room temperature. After being washed with PBS, cells were incubated with fluor-labeled secondary antibodies for 30 min. These included donkey-anti-goat IgG Alexa Fluor 488 (1:400) and donkey-anti-mouse IgG Alexa Fluor 568 (1:400) from Life Technologies. After cover glasses were washed in PBS, a drop of DAPI containing Fluoromount-G (Southern Biotech) was added to the cells. Cover glasses were placed on glass microscope slides. Microscopy was conducted with a Zeiss Axio Imager Z2 fluorescence microscope equipped with an ApoTome slider. Images were obtained with ZEN 2012 software (Zeiss) and processed with Photoshop CS4 (Adobe Systems) and freely available Fiji software.

Analysis of HS, Dermatan Sulfate, and Chondroitin Sulfate

GAG concentrations were determined in serum, urine, and fibroblasts as described previously.[40,41] In brief, we made homogenates from fibroblasts by disrupting the cells in PBS with a Vibra-Cell sonicator (Sonics & Materials). Protein concentrations were measured in whole-cell lysates as described by Lowry et al.[42] To obtain GAG disaccharides, we enzymatically digested 50 μL serum, 50 μL urine, or 25 μg fibroblast protein in a mixture containing 100 mM NH_4Ac (pH 7.0), 10 mM $Ca(Ac)_2$, 2 mM DTT, 5 mIU each of heparinase I, II, and III, and 50 mIU chondroitinase B or 50 mIU chondroitinase ABC in a final volume of 150 μL. After 2 hr of incubation at 30°C, 15 μL of 150 mM EDTA (pH 7.0) was added along with 125 ng of the internal standard, 4UA-2S-GlcNCOEt-6S (HD009, Iduron), and the reaction was stopped and boiled for 5 min for protein denaturing. The reaction mixture was centrifuged at 20,000 × *g* for 5 min at room temperature. Subsequently, the supernatant was applied to an Amicon Ultra 30K centrifugal filter (Millipore) and centrifuged at 14,000 × *g* for 15 min at 25°C. The filtrate was stored at 20°C until analysis. HS, dermatan sulfate (DS), and chondroitin sulfate (CS) levels were quantified on a Waters Quattro Premier XE (tandem) mass spectrometer (Waters Corporation) coupled to an Acquity UPLC system (UPLC-MS/MS) with a Thermo Hypercarb HPLC column (100 × 2.1 mm, 5 μm) and a mobile phase consisting of 10 mM NH_4HCO_3 (pH 10). Disaccharides were eluted with an acetonitrile gradient of 0%–20% for 2.5 min, held at 20% for the next 2.5 min, and equilibrated for 2 min at 0% before the next injection; the flow rate was 0.2 mL/min, and the total run time was 7.1 min. All disaccharides were detected and quantified in multiple-reaction-monitoring acquisition mode with the transitions m/z 378.1 > 175.1 for D0A0, 458.0 > 299.9 for D0a4, 378.0 > 175.0 for D0a0, and 458.0 > 97.0 for D0a6 (according to the nomenclature of Lawrence et al.[43]) and 472.0 > 97.0 for the 4UA-2S-GlcNCOEt-6S internal standard. The concentration of each disaccharide was calculated with a calibration curve for each of the disaccharides.

All samples were digested and analyzed in duplicate. For each subject, all serum and urine GAG levels were compared with those of age-matched control individuals (n = 4). The normal range for each GAG was defined as the mean ± 2 SDs of the control samples.

Results

Clinical Report

We report on nine affected individuals from five unrelated families affected by neuro-immuno-skeletal dysplasia syndrome. Families A and B were consanguineous, suggesting autosomal-recessive inheritance of the disorder (Figure 2A, Table 1, and Tables S1 and S2). Family C was from a geographically isolated district in Colombia (South America) and possibly had a distant degree of consanguinity. Family D was the offspring of families who had lived for several generations in two small neighboring Portuguese villages. Family E was of Indian descent and had no history of consanguinity.

All nine affected individuals presented with various skeletal dysplasias. In four families (A and C–E), X-rays revealed severe platyspondyly leading to disproportionate stature (Figure 1). Lumbar gibbus and kyphoscoliosis were observed in families C and D, respectively. Three individuals (from families D and E) had cervical malformations and a hypoplastic odontoid peg with cervical instability. Short stature was also present in families A and B but appeared to be the result of limb shortening. Metaphyseal abnormalities of the long bones were found in families A and E, whereas families B–D showed epiphyseal abnormalities (Figure 1). Brachydactyly was observed in affected individuals from families A, B, and D. In addition to showing skeletal abnormalities, all affected individuals in families B and C had intellectual disability (ID). This could not be assessed for individuals A:II-1, E:II-1, and E:II-2 because of their early death at 7 weeks, 6 months, and 10 months of age, respectively. Both siblings of family B were severely disabled and unable to speak and are currently wheelchair bound. Dysmorphic facial features were non-discriminatingly mild but included coarse facial features, a prominent

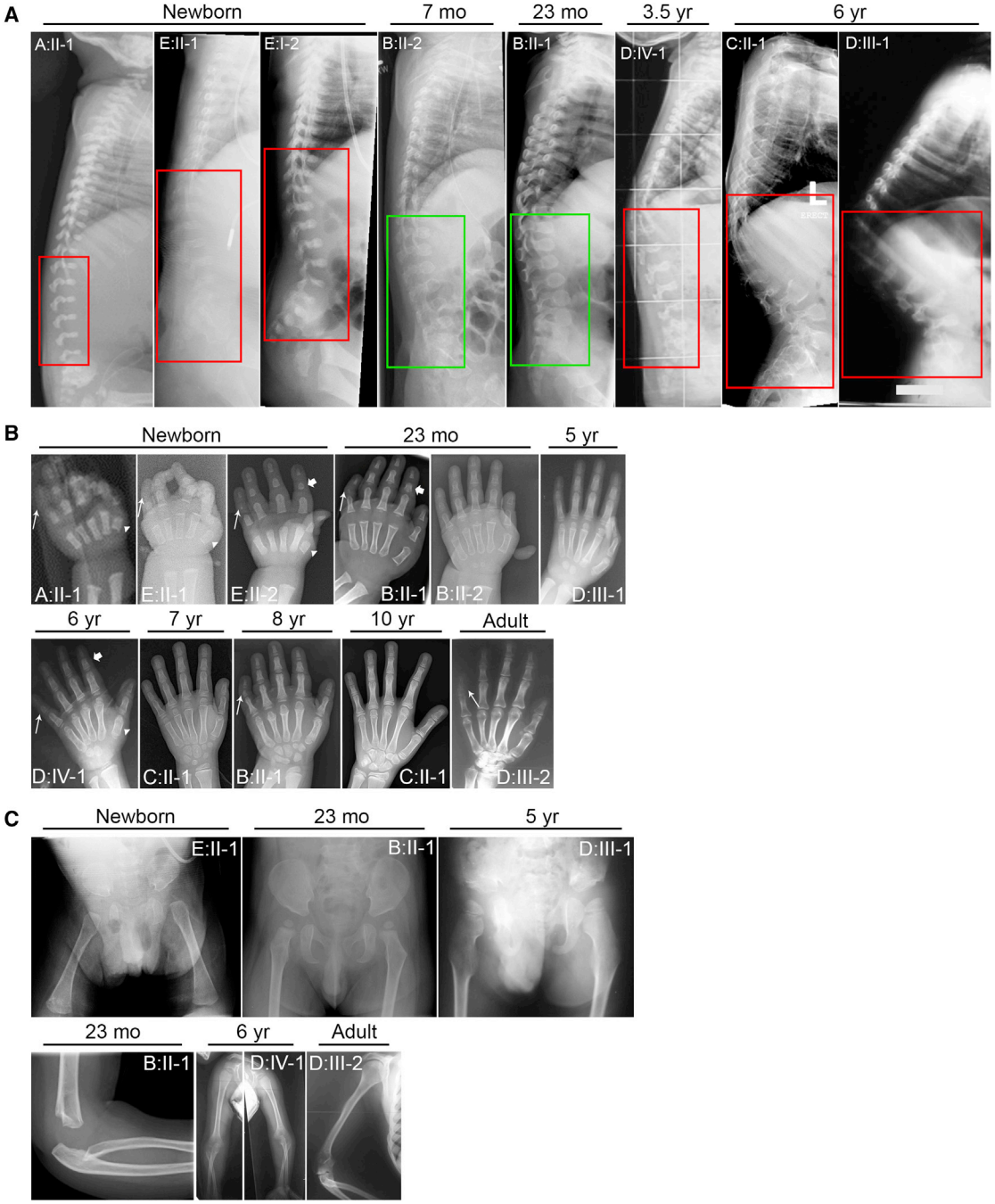

Figure 1. Clinical Features of the Skeleton of Families A–E

(A) Lateral spine radiographs arranged chronologically. Most affected individuals show severe platyspondyly (red boxes) with progressively severe kyphosis with increasing age (visualized for C:II-1, D:III-1, and D:IV-1); however, the affected siblings of family B do not (green boxes). Affected individual C:II-1 shows an additional abnormality of absent ossification of the anterior parts of the vertebral bodies in the upper lumbar region. Furthermore, wide intervertebral spaces are visible, and the vertebral bodies show some posterior constriction giving a pear shape.

(B) Hand radiographs arranged chronologically. Up to the age of about 6 years, there is a delay in carpal bone ossification. The first metacarpals (arrowheads) and the second middle phalanges (broad arrows) are short. The fifth middle phalanges are short or absent in A:II-1, E:II-1, and E:II-2 (newborns). Affected individual B:II-2 has soft tissue preaxial polydactyly.

(C) The pelvic radiographs show a variable degree of sloping acetabula with shallow lateral notches, coxa valga, and small capital femoral epiphyses. Elbow radiographs show dislocated radial heads with dysplastic radial heads.

nose, and full cheeks in almost all affected individuals (Figure S1). A single palmar crease was also observed in six of nine affected individuals. A striking phenotype present in three of the five families was T-cell-negative SCID. Affected individuals from families A and B showed a lack of T cells, whereas B cell numbers were normal (Figure 4).

Family E showed idiopathic $CD4^+$ lymphopenia and an absolute lack of naive T cells (both $CD4^+CD45RA^+$ and $CD8^+CD45RA^+$ T cells were missing). In families B and E, a typical skin rash prompted further evaluation of the blood cells. Maternal T cells were excluded, and the oligoclonal T cell reaction found in the presence of eosinophilia was compatible with an Omenn-like presentation of SCID.[1,2] Worth mentioning are also the liver cysts seen in affected individuals from families A and E. Although the phenotypes were widely variable and partly contrasting (e.g., severe versus no ID, severe versus mild platyspondyly, and epiphyseal versus metaphyseal changes), all major malformations and features occurred in three organ systems only: the immune system, the skeleton, and the neurological system. All together, we classify these five families as having phenotypic variability of an EXTL3-related neuro-immuno-skeletal dysplasia phenotype. The affected individuals from families A and E died in early infancy, whereas the others are currently between 2 and 38 years of age. Individual III-1 from family D died at 30 years of age from a unknown cause. Table 1 gives an overview of the most affected organ systems in all affected individuals. Detailed case reports and clinical data for each affected individual can be found in the Supplemental Note.

WES

Massive parallel sequencing of genomic DNA of nine affected individuals from five unrelated families was performed in four different centers (Figure 2A). WES data were filtered according to a recessive disease model given that families A and B showed consanguineous bonds and families B, D, and E each had more than one affected individual. The severity of the phenotype, especially in families A and E, suggests that the disease is caused by a rare genetic mutation. We therefore prioritized homozygous and compound-heterozygous variants, nonsense variants, and variants with a phyloP score > 2.7 given that the majority of annotated variants in the Human Gene Mutation Database have such scores.[45] After application of these rules in family A, only 2 of 37 candidate variants segregated with the disease in the family (Table 2 and Table S3). These two mutations were homozygous missense mutations in *EXTL3* (c.1537C>T [p.Arg513Cys] [GenBank: NM_001440.3]) and *CHST9* (MIM: 610191; c.1133A>G [p.Asn378Ser] [GenBank: NM_031422]) (Figure 2B). Left with two candidate genes, we made use of GeneMatcher, a web-based tool for researchers and clinicians working on identical genes.[17] A match was found in four independent families from different centers. WES data from these families revealed likely pathogenic homozygous missense mutations in *EXTL3*. Data from these families also revealed one or more genes carrying biallelic variants that segregated with the disease; however, in each family the variant in *EXTL3* was the most likely candidate given the position and predicted impact of the variant together with the segregation analysis (Table 2 and Tables S3–S7). In total, we found four homozygous missense mutations: c.1382C>T (p.Pro461Leu), c.1537C>T (p.Arg513Cys), c.1970A>G (p.Asn657Ser), and c.2008T>G (p.Tyr670Asp). Variant analysis in the ExAC Browser showed that homozygous non-synonymous alterations in coding regions of *EXTL3* are not tolerated. Only one such alteration was present (c.1324G>C [p.Val442Leu]), and it is predicted to be tolerated by SIFT prediction software (analysis performed in October 2016). Furthermore, variants p.Arg513Cys and p.Tyr670Asp were both absent from the ExAC Browser. The other two variants, p.Pro461Leu and p.Asn657Ser, were present only in a heterozygous state with detected MAFs of 1.6×10^{-5} and 5.8×10^{-5}, respectively. CNV analysis, including the SNP array in family B, did not reveal any likely pathogenic alterations (data not shown).

All together, we found homozygosity for four missense mutations in *EXTL3* in five unrelated families as a cause of a recessive form of neuro-immuno-skeletal dysplasia.

Validation of EXTL3 Antibody

In order to validate the specificity of the antibody targeting EXTL3, we made use of CRISPR/Cas9 techniques to knock out EXTL3 in HEK293T cells and study the protein lysate on western blotting. A band of approximately 130 kDa was clearly visible in lanes 1, 2, and 4, corresponding to cell lysates from HEK293T cells transfected with sgRNA 1, sgRNA 2, and the empty vector pLentiCRISP v.2, respectively. The absence of a band in lane 3 corresponding to cell lysates from HEK293T cells transfected with sgRNA 3 validates the specificity of the antibody targeting EXTL3 (goat, AF2635, R&D Systems) (Figure 3D).

EXTL3 Is Present during Early T Cell Development

Investigation of immune cells detected a complete or nearly complete absence of T cells but normal counts of B and natural killer (NK) cells in affected individuals from three families (A, B, and E; Table 3). Only a limited number of gene defects are known to result in T-negative SCID.[1,2] The disease is most often caused by a lack of signaling of the T cell receptor to propagate the development of thymocytes toward the single $CD4^+$ and $CD8^+$ T cell stage.[46] There is no published information about the actual level of EXTL3 in T cells. To elucidate the disease mechanism underlying the T cell deficiency seen in three of these five families, we studied the levels of EXTL3 in both T and B lymphocytes of normal control samples. EXTL3 was not observed by western blotting in circulating T or B lymphocyte cell types (Figure 3A). After strong activation by a combination of CD3 and CD28 during culture for 6 days into T cell blasts ($CD4^+CD27^-$ or $CD8^+CD27^-$), low levels of EXTL3 were detected (Figure 3A). It was far less, if any at all, for activated B cells differentiating for 6 days into plasmablasts ($CD38^+CD138^+$) (Figure 3A).

These findings suggest that the effect of the selective T cell defect that we observed in EXTL3 deficiency could depend on the early protein levels during hemato- and/or lymphopoietic development before the circulating stage in peripheral blood. Indeed, EXTL3 was demonstrated at

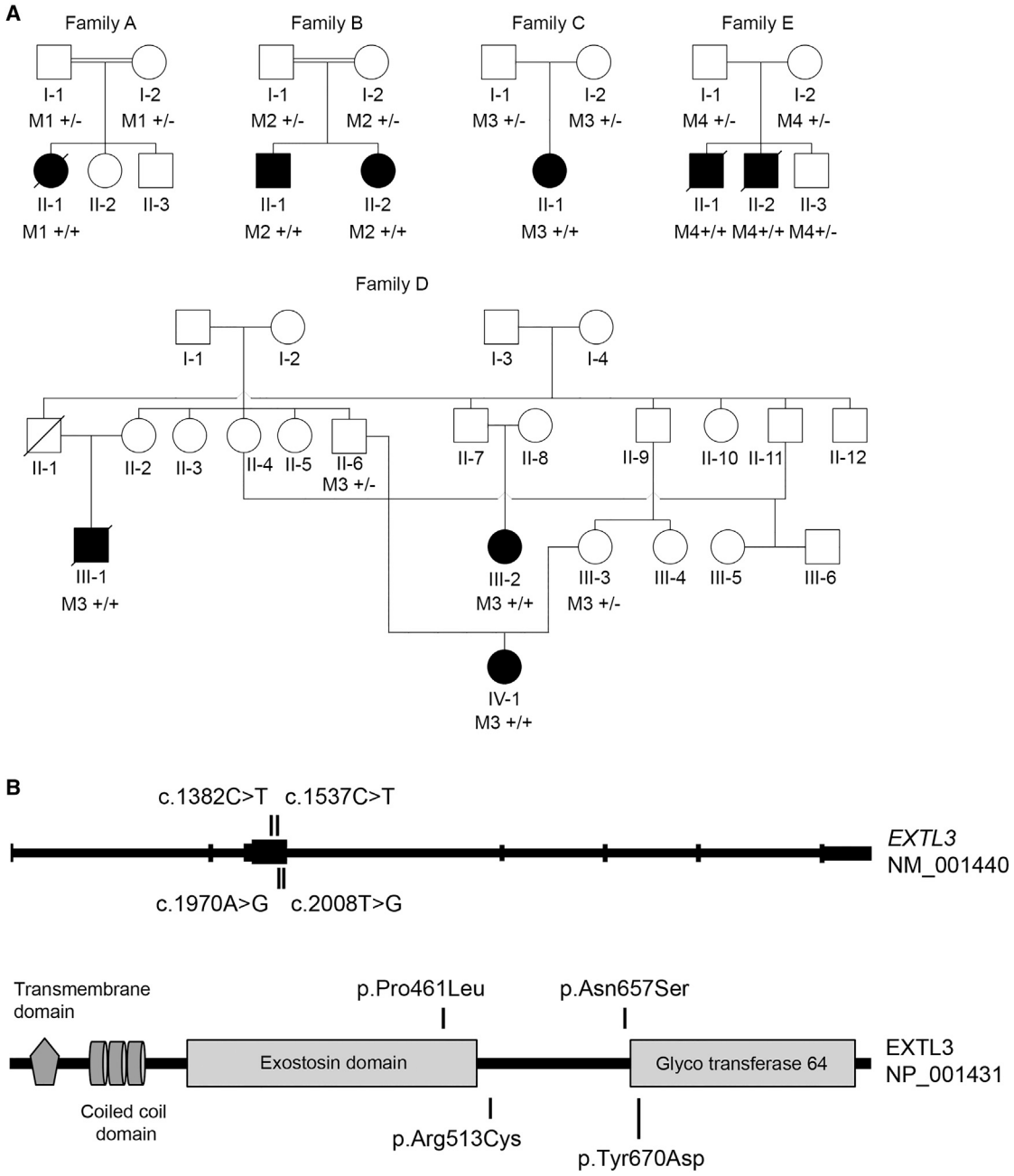

Figure 2. Four Homozygous Missense Mutations in *EXTL3* in Five Unrelated Families
(A) Pedigrees of five affected families. All affected individuals carry homozygous missense mutations in *EXTL3* (GenBank: NM_001440.3). In family A, II-1 is homozygous for c.1537C>T (M1). In family B, II-1 and II-2 are homozygous for c.2008T>G (M2). In families C and D, c.1382C>T segregates with disease. In family E, c.1970A>G (M4) segregates with disease.
(B) Schematic overview of *EXTL3* and the corresponding protein (GenBank: NP_001431) shows the position of the missense mutations and protein changes. All four mutations are in exon 3. EXTL3 consists of two annotated domains: a transmembrane domain (amino acids 29–51) and a coiled-coil domain (amino acids 86–148). In addition, there are two predicted Pfam domains: a conserved EXT domain (amino acids 190–500) and a glycosyl transferase family 64 domain (amino acids 663–904) conserved between enzymes that catalyze the transfer reaction of *N*-acetylglucosamine and *N*-acetylgalactosamine.[44]

the protein level in purified $CD34^+$ hematopoietic stem cells (HSCs) (Figure 3B), as well as in the immature (leukemic) T cell lines (Figure 3A). As was expected from the analysis of T and B cell subsets from blood or upon in vitro activation, none of the more mature T or B cell lines or any additional hematopoietic cell lines tested (including Jurkat cells, Ramos cells, Epstein-Barr virus B cell blasts, KG1a cells, HL-60 cells, and U937 cells) demonstrated any EXTL3 at the protein level (Figure 3A).

To assess thymic tissue from neonates for the level of EXTL3, we fractionated the thymocytes into early double-negative, double-positive, and late single-positive

Table 2. Causative *EXTL3* Mutations Detected by WES in the Five Families

Family	Chromosome	hg19 Position	*EXTL3*[a] Variant	Amino Acid Change	ExAC Browser Frequency	PhyloP Score	SIFT Score	PolyPhen-2 Score
A	8	g.28575113	c.1537C>T	p.Arg513Cys	NP	6.238	0	1
B	8	g.28575584	c.2008T>G	p.Tyr670Asp	NP	7.984	0	1
C and D	8	g.28574958	c.1382C>T	p.Pro461Leu	1.65×10^{-5}	7.727	0	1
E	8	g.28575546	c.1970A>G	p.Asn657Ser	5.80×10^{-5}	9.206	0	1

NP means not present in the database.
[a]GenBank: NM_001440.3.

thymocytes. EXTL3 was observed in all fractions, including the single-positive $CD4^+$ or $CD8^+$ thymocytes (Figure 3B).

Upon immunohistochemistry staining of thymus tissue from a normal neonate obtained at post-mortem examination (cause of death: asphyxia), EXTL3 showed moderate localization throughout the thymus in both the cortical and extramedullary niches (Figure 3C). These findings suggest that the level of EXTL3 is downregulated when T cells enter the circulation.

By determining the immunophenotype of circulating B and T cells in families A and B, we confirmed the T cell selective effect in the *EXTL3*-mutated individuals with a so-called T-negative SCID phenotype. Skewing of the distribution of the T cell memory subset toward a highly differentiated phenotype was observed in individual B:II-1, but not in the transplanted sibling, B:II-2 (Figure 4A). Upon stimulation with anti-CD3 and anti-CD28, the proliferative response of both $CD4^+$ and $CD8^+$ T cells in individual B:II-1 was impaired in comparison with that of the transplanted sibling (B:II-2) and healthy control individuals (Figure 4C). Furthermore, the T cells in individual B:II-1 were unable to induce B cell proliferation (Figure 4C).

To exclude a functional B cell defect due to the early lack of EXTL3 at the HSC and common lymphoid progenitor (CLP) stages within the bone marrow, we generated plasmablasts and tested antibody release into the supernatant upon stimulation with CpG and IL-2 in families A and B. The distributions of memory B cell subsets were normal for their age (Figure 4A). Functionally, these data showed normal B cell activation and plasmablast formation (low-normal for age) with IgM and IgG release in individual A:II-1 (Figures 4B and 4D–4F). The low in vitro IgG production in individual B:II-2 can be ascribed to the fact that she had been transplanted only 1 year earlier with a few circulating donor memory B cells at this stage, whereas the older sibling (B:II-1) showed 5% $CD27^+$ memory B cells, plasmablast formation, and production of IgG and IgM (Figures 4B and 4D–4F).

On the other hand, in one of the two families affected by the p.Pro461Leu variant and not prone to infections (family C), normal lymphocyte counts were found in initial white blood cell differentials. We confirmed that the lymphocyte numbers, maturation, subset distribution (naive, central-memory, and effector-memory T cells; naive, non-switched, and switched memory B cells; and NK cells), and proliferative capacity were completely normal (Figure S2).

Together, these immunological data indicate that a severe T cell defect is most apparent, although variable, whereas the other hematopoietic cell lineages seem to develop normally.

EXTL3 Mislocalizes in Fibroblasts Derived from Affected Individuals

In order to determine the effects of the missense variants identified herein, we compared EXTL3 localization in fibroblasts derived from A:II-1, B:II-1, and B:II-2 with that in cells from two unaffected control individuals by immunofluorescence microscopy. Overlap between the EXTL3 signal and that of GM130, a Golgi marker, indicates that EXTL3 localized to the Golgi complex in control fibroblasts. In contrast to the control cell lines, fibroblasts derived from individual A:II-1 did not show any EXTL3 in the Golgi complex (Figure 5), further supporting the causality of *EXTL3* mutations in this individual. However, we could detect EXTL3 in the Golgi complex in fibroblasts from affected individuals in family B. We suspect that the p.Arg513Cys variant, which is located near the EXT domain (Figure 2B), causes degradation of EXTL3 and leads to its absence from the Golgi complex in cells from individual A:II-1. On the other hand, we speculate that the p.Tyr670Asp variant detected in family B does not affect EXTL3 localization but rather disrupts its GlcNAc transferase activity, given that this variant lies in the glycosyl transferase family 64 region of the protein (Figure 2B).

HS Levels Are Altered in Material Derived from Affected Individuals

We then determined whether the identified mutations in affected individuals A:II-1, B:II-1, B:II-2, C:II-1, D:IV-1, and E:II-1 alter GAG synthesis, given that EXTL3 is known to be essential for HS biosynthesis.[9] GAG concentrations were measured in serum and urine of A:II-1, B:II-1, and B:II-2 and compared with those in age-matched control individuals (Figures 6B and 6C). In addition, the GAG concentrations were measured in fibroblasts from all families. Because the levels of most disaccharides were below the limit of quantification in several samples, we present only the results for the most abundant disaccharides for each GAG: D0A0 for HS, D0a4 for DS, and D0a6 and

Table 3. Lymphocyte Counts in Individuals with *EXTL3* Mutations and Pediatric Control Individuals

Individual	Age	$CD3^+$ T Cell (per μL)[a]	$CD3^+CD4^+$ T Cells (per μL)	$CD3^+CD8^+$ T Cells (per μL)	$CD19^+$ B Cells (per μL)	$CD56^+$ NK Cells (per μL)	IgG (g/L)	IgA (g/L)	IgM (g/L)
A:II-1	NA	0	0	0	1436	279	1.0	<0.1	0.3
B:II-1	7 years	367 (25%)	157 (8%)	210 (11%)	656 (34%)	262 (13%)	5.65	0.39	0.24
	8 years	488 (25%)	176 (9%)	293 (15%)	819 (42%)	585 (30%)	4.52	0.29	<0.2
B:II-2[b]	3 months	2442 (51%)	2442 (51%)	0	1436 (30%)	575 (12%)	12.9	0.2	2.5
C:II-1	12 years	819 (44%)	348 (19%)	221 (12%)	557 (30%)	453 (25%)	NA	NA	NA
D:III-1	NA	NA	NA	NA	NA	NA	NA	NA	NA
D:III-2	NA	NA	NA	NA	NA	NA	NA	NA	NA
D:IV-1	12 years	600 (36%)	382 (23%)	206 (12%)	538 (32%)	513 (31%)	NA	NA	NA
E:II-1[c]	2.5 months	1800 (40%)	500 (11%)	1310 (25%)	2030 (45%)	360 (8%)	<1.6	<0.4	0.5
E:II-2	9 months	10 (0.2%)	0	0	1950 (69%)	760 (27%)	4.7	<0.06	0.11
Pediatric control individuals	<2 years	700–1,500	400–900	400–1,100	300–1,500	50–400	5–10	0.7–1.5	0.3–1.2

Parentheses show the percentage of the lymphocyte subtype within the total lymphocyte count. NA means no data available.
[a]All values were obtained before hematopoietic stem cell transplantation (HSCT).
[b]IgG before administration of intravenous immunoglobulins and before HSCT. Ig subclasses (g/L): IgG1, 11.9; IgG2, 1.69; IgG3, 0.57; IgG4, 0.19.
[c]Already developed Omenn syndrome.

D0a0 for CS. The concentrations of these disaccharides strongly correlate with total GAG concentrations.[40]

HS concentrations in fibroblasts of all affected individuals except C:II-1 were markedly lower than those in control fibroblasts. For the affected individuals in family B, the HS concentrations were also reduced in serum and urine, whereas both parents in family B had serum HS concentrations within the normal range. Surprisingly, for individual A:II-1, HS concentrations were normal in serum and urine.

DS concentrations, measured by the disaccharide D0a4, showed more variable results. They were within the normal range in fibroblasts from families B and D, reduced in families A and E, and increased in family C. In serum and urine, they were elevated in all three affected individuals studied (A:II-1, B:II-1, and B:II-2). The DS concentration was also elevated in the serum of the father in family B (B:I-1) and was below the limit of detection in the serum of the mother (B:I-2).

The CS concentrations in urine and serum showed an increase in the non-sulfated CS disaccharide D0a0. The other CS disaccharide, D0a6, was elevated only in the urine and serum of individual B:II-2, whereas this disaccharide was in the normal range in the samples from both A:II-1 and B:II-1.

In summary, although the findings differ among affected individuals and among the biological materials investigated, the results show abnormal glycosylation patterns in the affected individuals with generally lower HS and elevated DS and CS concentrations.

Discussion

In this study, we identified homozygous missense mutations in *EXTL3* in nine neuro-immuno-skeletal dysplasia individuals with a variable phenotype from five unrelated families. EXTL3 and the other four EXT family members are involved in the biosynthesis of HS.[9,47] Specifically, EXTL3 regulates the initiation of HS chain formation by enzymatically catalyzing GlcNac binding to the GAG linkage region of a specific protein.[9] This process is crucial in early development, given that complete *Extl3* knockdown in mice is lethal around 9 days postcoitum.[11] Zebrafish with the mutant *tm70g* allele in *extl3* (previously *boxer*) have been reported to have penetrant pectoral fin and jaw phenotypes and lack swim bladders, which can be completely rescued with wild-type *extl3*.[48] This phenotype could turn out to be comparable to the human one. Because the affected individuals reported in the current study survived past the neonatal period, we expect that homozygosity for the variants (p.Pro461Leu, p.Arg513Cys, p.Asn657Ser, and p.Tyr670Asp) leads to diminished EXTL3 activity. The mutations probably have different effects on EXTL3 function. This is supported by the immunofluorescence data (Figure 5), which showed that EXTL3 was absent from the Golgi complex only in fibroblasts derived from individual A:II-1, whereas it was still detectable in fibroblasts derived from siblings B:II-1 and B:II-2. The localization defect in A:II-1 could be explained by EXTL3 degradation due to the p.Arg513Cys variant in this family, whereas the variant in family B presumably affects the enzymatic function of EXTL3 without disrupting its localization to the Golgi complex. The latter speculation is based on the presence of the p.Tyr670Asp variant in the glycosyl transferase family 64 domain of EXTL3 (Figure 2B). The pathophysiological effects of the EXTL3 variants identified in families C and D are clearly different from those in families A, B, and E; further functional

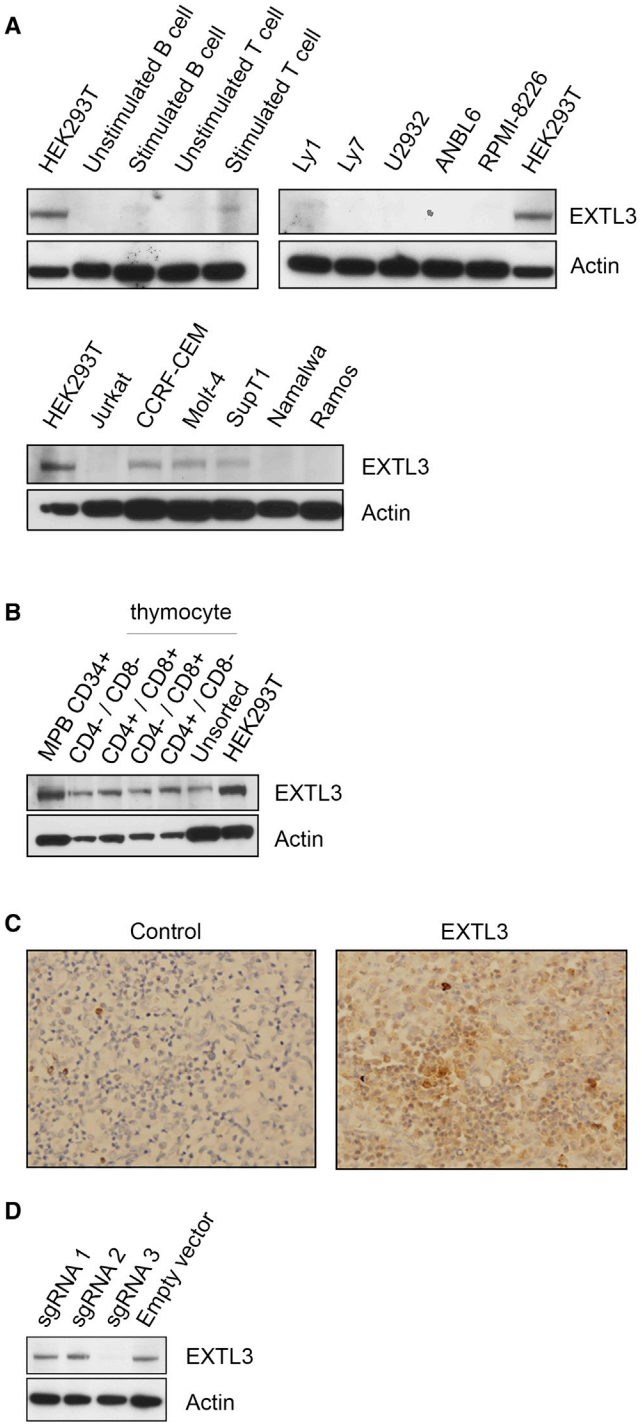

Figure 3. EXTL3 Levels in T and B Lymphocyte Cell Lines

(A) EXTL3 was absent in all B cell lymphoma cells, myeloid cells, or circulating B and T lymphocyte cell lines. However, strong T cell stimulation seemed to induce low levels of EXTL3.

(B) Purified $CD34^{+}$ hematopoietic stem cells and thymocyte cells were positive for EXTL3. This was true for early double-negative, double-positive, and late single-positive thymocyte cells.

(C) Immunohistochemistry staining of normal neonate tissue for localization of EXTL3 shows moderate localization throughout the thymus.

(D) Validation of EXTL3 antibody. The EXTL3 antibody shows a band for cells transfected with sgRNAs 1 and 2 and the empty vector, indicating the presence of EXTL3 in the cell lysate. Upon transfection with sgRNA 3, an EXTL3 knockout cell line was obtained; no band was visible, indicating the specificity of the antibody.

reconstitution assays should formally prove the effects on functional activity. The p.Pro461Leu variant detected in families C and D is located within the EXT domain. This domain is shared among the EXT family members and appears to be associated with skeletal phenotypes,[49] whereas the severe immunological phenotype seems to be associated with improper GAG modifications that rely on intact function of EXTL3. It remains unclear which proteins, either cellular or extracellular,[50] will be most affected by the perturbed GAG production in individuals with EXTL3 variants.

All four described EXTL3 variants show an effect on GAG concentrations, whereas all HS concentrations are generally lower and both DS and CS concentrations are elevated. This supports the hypothesis that improper function of EXTL3 leads to unbalanced GAG synthesis and results in less HS and more DS and CS. The only unexpected findings were normal HS concentrations in the urine and serum of individual A:II-1, who did have markedly reduced HS concentrations in fibroblasts, and normal HS concentrations in the urine and serum of affected individual C:II-1. At the moment, we cannot explain these results, and they require further investigation.

Despite the common neuro-immuno-skeletal dysplasia phenotype of the affected individuals, the presence or absence of the concomitant SCID phenotype clearly suggests phenotypic variability (with an immense impact on survival) between the reported families. The skeletal phenotype is mainly spondyloepy(meta)physeal dysplasia, overlapping the growing clinical spectrum of other linkeropathies (e.g., associated malformations, dislocations, etc.). Linkeropathies are associated with a short trunk or short stature resulting from spinal malformations and platyspondyly, as well as joint laxity, dislocations, and osteoporosis. Furthermore, extra-skeletal features such as ID, facial dysmorphisms, and congenital anomalies are common in linkeropathies and are also present in the affected individuals described here. Motor development appears to be seriously affected by the EXTL3-related neuro-skeletal features in most of the reported affected individuals (Table 1 and Table S1). ID appears not to be a constant feature. Whether these phenotypic differences are due to the different positions of the mutations in the gene or caused by other unknown modifiers remains unclear. That said, it is worth noting that variable penetrance of a T cell immunodeficiency, as observed in the five presented families, has previously been reported in SIOD and CHH (GeneReviews and Ridanpää et al.[4]).

With respect to the SCID phenotype in three families, we have demonstrated that the EXTL3 defect is at the level of early T cell development in the thymus. According to current models of hematopoiesis, lymphoid-primed multi-potent progenitors ($Lin^{-}Sca\text{-}1^{+}c\text{-}Kit^{+}CD34^{+}Flt3^{hi}$)

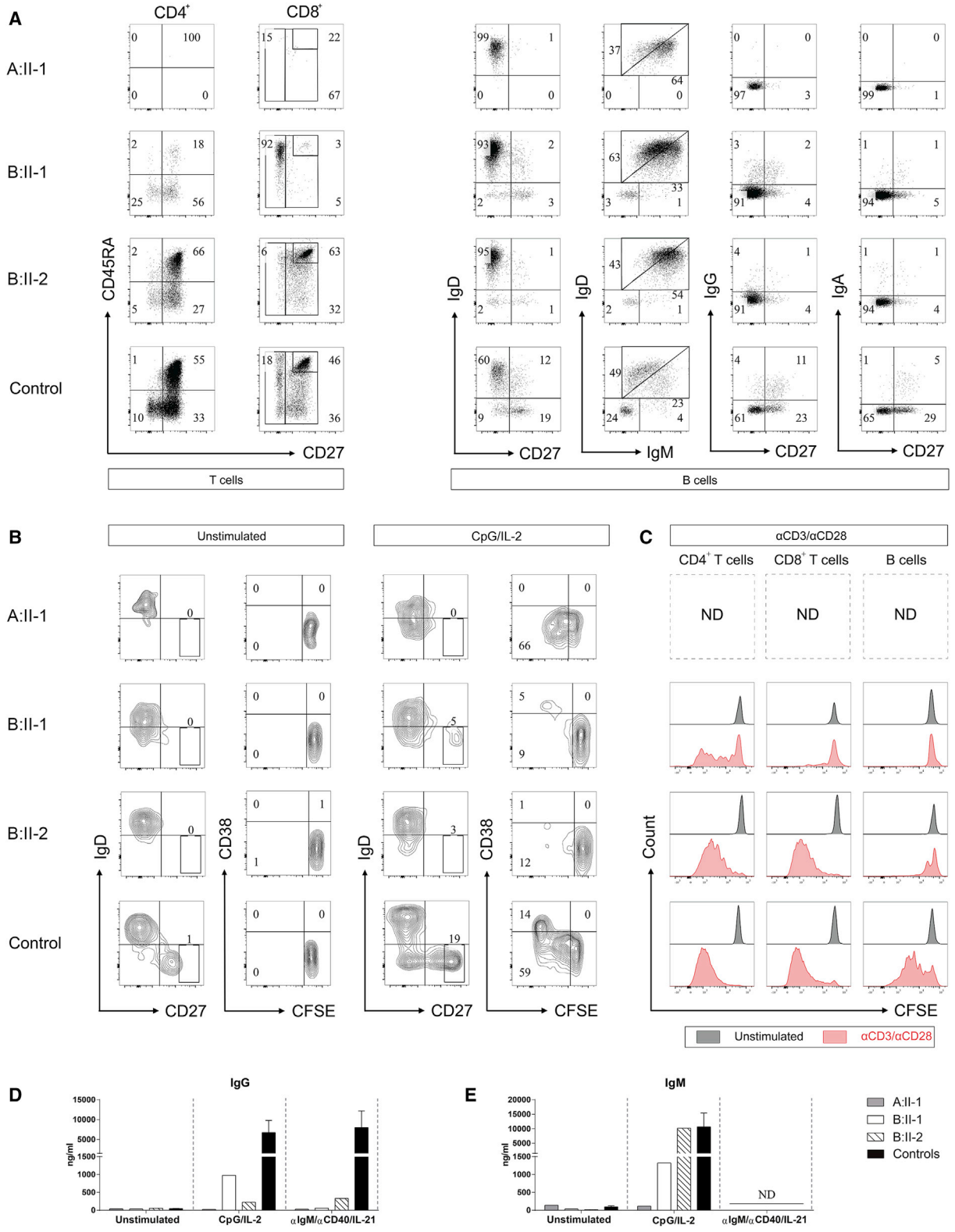

Figure 4. Immunophenotype and In Vitro Proliferation, Plasmablast Formation, and Immunoglobulin Production
Data are shown for individuals A:II-1, B:II-1, and B:II-2 and a healthy adult control individual.
(A) T cell subsets gated on $CD3^{+}CD4^{+}$ or $CD3^{+}CD8^{+}$ lymphocytes and B cell subsets gated on $CD19^{+}CD20^{+}$ lymphocytes. Numbers indicate percentages in the corresponding gates.
(B) CFSE-labeled PBMCs were cultured with either medium or CpG and IL-2 and were gated on $CD19^{+}CD20^{+/-}$ lymphocytes. Gates were set for either $CD27^{bright}$ (left) or $CFSE^{+/-}$ and $CD38^{+/-}$ (right) B cells for analysis of cell division and plasmablast formation.

(legend continued on next page)

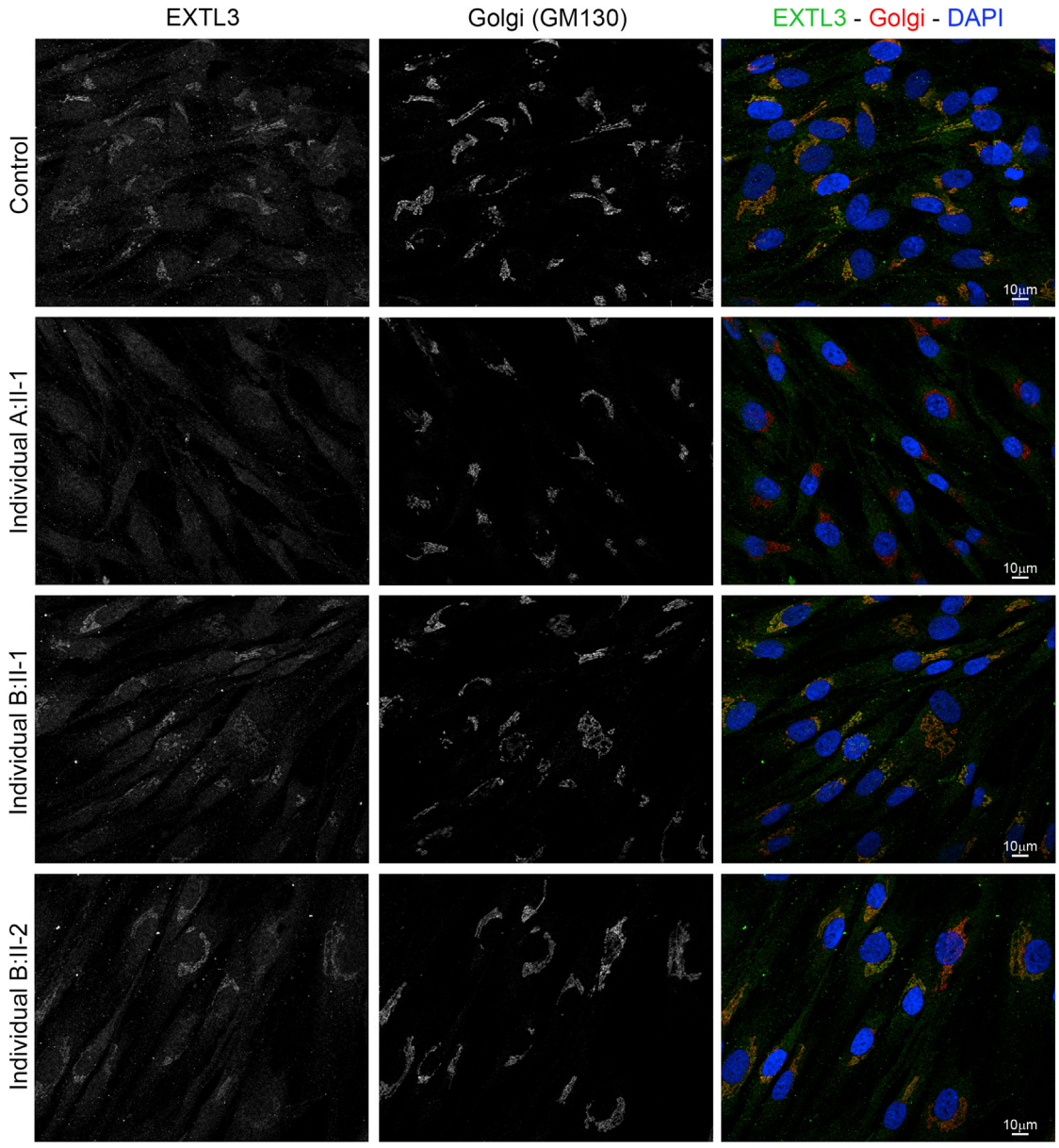

Figure 5. Localization of EXTL3 to the Golgi Complex Is Lost in p.Arg513Cys Mutated Cells
The localization of EXTL3 in fibroblasts derived from affected individuals is compared with that of two healthy control individuals. The cells were stained for EXTL3 (green), Golgi marker GM130 (red), and DAPI for the cell nucleus (blue). The localization of EXTL3 to the Golgi complex seen in control fibroblasts was lost in cells derived from affected individual A:II-1, but not in fibroblast cell lines from affected siblings B:II-1 and B:II-2. Scale bars represent 10 μm.

and common myeloid progenitors ($Lin^{-}Sca\text{-}1^{+}c\text{-}Kit^{+}CD34^{+}CD41^{hi}$) establish an early branch point for separate lineage commitment from hematopoietic stem cells. Although the common lymphoid progenitor compartment seemed to be involved, our further exploration of this cellular complexity in immunological development suggested that EXTL3 plays an important role at the thymic stage of T cell development. It has been described that HSPGs influence hematopoietic progenitor cell development,[13,14] in keeping with our finding that EXTL3 was most abundant in hematopoietic stem cells and early progenitor cells.

Hematopoietic stem cell transplantation (HSCT) in one of the EXTL3-deficient SCID individuals resulted in

(C) CFSE-labeled PBMCs were cultured with either medium or anti-CD3 and anti-CD28 and were gated on $CD3^{+}CD4^{+}$ or $CD3^{+}CD8^{+}$ T lymphocytes and $CD19^{+}CD20^{+/-}$ B lymphocytes for analysis of direct (T cell) or indirect (B cell) proliferation upon TCR stimulation. ND means not determined.
(D and E) Levels of IgG and IgM were determined by ELISA in the supernatants after 6 days of culture with medium, CpG and IL-2, or a combination of anti-IgM, anti-CD40, and IL-21. Error bars indicate SEM (n = 3).

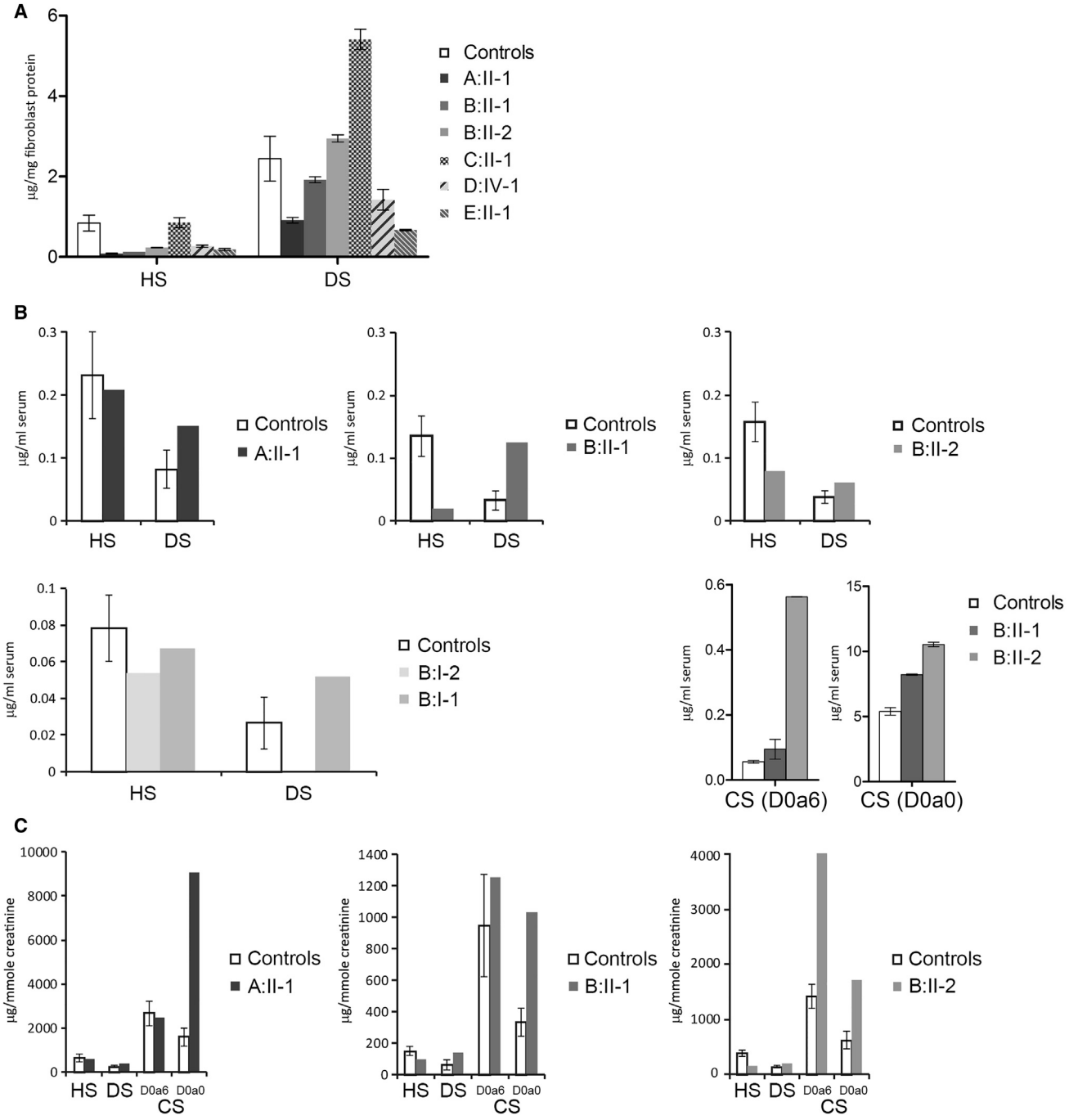

Figure 6. Mutations in *EXTL3* Affect Glycosaminoglycan Concentrations

GAG concentrations in urine, serum, and fibroblasts from affected individuals and age-matched control samples. Concentrations of D0A0 for heparan sulfate (HS), D0a4 for dermatan sulfate (DS), and D0a6 (sulfated) and D0a0 (non-sulfated) for chondroitin sulfate (CS) are shown. Error bars indicate SD.

(A) GAG concentrations in fibroblasts. HS concentrations were reduced in fibroblasts from all affected individuals except C:II-1. DS concentrations were within the normal range for the affected family members of family B and D:IV-1, increased in C:II-1, and reduced in A:II-1 and E:II-1.

(B) GAG concentration in the serum from affected individuals and both parents of family B. HS concentrations were normal in affected individual A:II-1 and in both parents of family B (B:I-1 and B:I-2) but were decreased in the siblings of family B (B:II-1 and B:II-2). DS concentrations were elevated in all affected family members of families A and B, as well as in parent B:I-1. The non-sulfated CS concentration was elevated in individuals B:II-1 and B:II-2, and the sulfated CS concentration was markedly increased in B:II-2.

(C) GAG concentrations in urine. HS concentrations for A:II-1 were normal but were decreased in both B:II-1 and B:II-2. DS was elevated in all three affected individuals. The non-sulfated CS concentration was elevated in all affected individuals, whereas D0a6 was elevated only in B:II-2.

complete recovery of normal T cell development without affecting either the non-hematopoietic defects or the abnormal GAG findings in blood and urine samples.

In summary, we have presented nine individuals affected by a neuro-skeletal dysplasia phenotype in five independent families. The immunological features are variable—three of five families presented with a severe T cell immunodeficiency caused by a lack of $CD4^+$ and $CD8^+$ T cells. WES analysis revealed that all affected individuals harbored mutations in *EXTL3*. A remedy for this disorder is not available, but the T-cell-negative (S)CID phenotype seen in five of the nine affected individuals presented here indicates that preventive measures should be taken against infections and that a HSCT procedure could cure the severe T cell defect in these individuals.

Supplemental Data

Supplemental Data include a Supplemental Note, two figures, and seven tables and can be found with this article online at http://dx.doi.org/10.1016/j.ajhg.2017.01.013.

Acknowledgments

We thank the families for participating in our study; all members of the clinical teams involved in the care of the described families; D. Braun, J. Lawson, and Dr. Hildebrandt for their screening effort; Dr. P. Meinecke for reviewing the X-rays; Dr. Dulce Quelhas and Dr. Lisa Woodbine for providing fibroblasts of affected individuals; Hanka Venselaar for helping with protein prediction models; and the Exome Aggregation Consortium and the groups that provided exome variant data for comparison. This study was partly funded by the Dutch Kidney Foundation (KOUNCIL consortium project CP11.18 to H.H.A.), Netherlands Organization for Health Research and Development (ZonMW Veni-91613008 to H.H.A.), Netherlands Organization for Scientific Research (NWO Vici-865.12.005 to R.R.), Center of Immunodeficiencies Amsterdam, and Fundação para a Ciência e Tecnologia (SFRH/BD/46778/2008). GOSgene at the University College London (UCL) Institute of Child Health is supported by the National Institute for Health Research Biomedical Research Centre (NIHR BRC) at Great Ormond Street Hospital for Children NHS Foundation Trust and UCL Institute of Child Health. This report is of independent research by the NIHR BRC Funding Scheme. The views expressed in this publication are those of the authors and not necessarily those of the NHS, NIHR, or Department of Health. Analysis of family C was performed by the Care4Rare Canada Consortium, funded by Genome Canada, the Canadian Institutes of Health Research, the Ontario Genomics Institute, Ontario Research Fund, Genome Quebec, and Children's Hospital of Eastern Ontario Foundation.

Received: November 1, 2016
Accepted: January 3, 2017
Published: January 26, 2017

Web Resources

1000 Genomes Project, http://www.internationalgenome.org/
Exome Aggregation Consortium (ExAC) Browser, http://exac.broadinstitute.org
GeneMatcher, http://genematcher.org
GeneReviews, Morimoto, M., Lewis, D.B., Lucke, T., and Boerkoel, C.F. (1993). Schimke Immunoosseous Dysplasia, https://www.ncbi.nlm.nih.gov/books/NBK1376/
Matchmaker Exchange, http://www.matchmakerexchange.org
NHLBI GO Exome Sequencing Project (ESP), https://esp.gs.washington.edu/drupal/
OMIM, http://www.omim.org/
PhenomeCentral, http://www.phenomecentral.org
RefSeq, http://www.ncbi.nlm.nih.gov/RefSeq
UniProt, http://www.uniprot.org/

References

1. Bousfiha, A., Jeddane, L., Al-Herz, W., Ailal, F., Casanova, J.L., Chatila, T., Conley, M.E., Cunningham-Rundles, C., Etzioni, A., Franco, J.L., et al. (2015). The 2015 IUIS Phenotypic Classification for Primary Immunodeficiencies. J. Clin. Immunol. *35*, 727–738.
2. Picard, C., Al-Herz, W., Bousfiha, A., Casanova, J.L., Chatila, T., Conley, M.E., Cunningham-Rundles, C., Etzioni, A., Holland, S.M., Klein, C., et al. (2015). Primary Immunodeficiency Diseases: an Update on the Classification from the International Union of Immunological Societies Expert Committee for Primary Immunodeficiency 2015. J. Clin. Immunol. *35*, 696–726.
3. Warman, M.L., Cormier-Daire, V., Hall, C., Krakow, D., Lachman, R., LeMerrer, M., Mortier, G., Mundlos, S., Nishimura, G., Rimoin, D.L., et al. (2011). Nosology and classification of genetic skeletal disorders: 2010 revision. Am. J. Med. Genet. A. *155A*, 943–968.
4. Ridanpää, M., van Eenennaam, H., Pelin, K., Chadwick, R., Johnson, C., Yuan, B., vanVenrooij, W., Pruijn, G., Salmela, R., Rockas, S., et al. (2001). Mutations in the RNA component of RNase MRP cause a pleiotropic human disease, cartilage-hair hypoplasia. Cell *104*, 195–203.
5. Boerkoel, C.F., Takashima, H., John, J., Yan, J., Stankiewicz, P., Rosenbarker, L., André, J.L., Bogdanovic, R., Burguet, A., Cockfield, S., et al. (2002). Mutant chromatin remodeling protein SMARCAL1 causes Schimke immuno-osseous dysplasia. Nat. Genet. *30*, 215–220.
6. Holmborn, K., Habicher, J., Kasza, Z., Eriksson, A.S., Filipek-Gorniok, B., Gopal, S., Couchman, J.R., Ahlberg, P.E., Wiweger, M., Spillmann, D., et al. (2012). On the roles and regulation of chondroitin sulfate and heparan sulfate in zebrafish pharyngeal cartilage morphogenesis. J. Biol. Chem. *287*, 33905–33916.
7. Izumikawa, T., Egusa, N., Taniguchi, F., Sugahara, K., and Kitagawa, H. (2006). Heparan sulfate polymerization in Drosophila. J. Biol. Chem. *281*, 1929–1934.
8. Kitagawa, H., Izumikawa, T., Mizuguchi, S., Dejima, K., Nomura, K.H., Egusa, N., Taniguchi, F., Tamura, J., Gengyo-Ando, K., Mitani, S., et al. (2007). Expression of rib-1, a Caenorhabditis elegans homolog of the human tumor suppressor EXT genes, is indispensable for heparan sulfate synthesis and embryonic morphogenesis. J. Biol. Chem. *282*, 8533–8544.
9. Kim, B.T., Kitagawa, H., Tamura, J., Saito, T., Kusche-Gullberg, M., Lindahl, U., and Sugahara, K. (2001). Human tumor suppressor EXT gene family members EXTL1 and EXTL3 encode alpha 1,4- N-acetylglucosaminyltransferases that likely are involved in heparan sulfate/ heparin biosynthesis. Proc. Natl. Acad. Sci. USA *98*, 7176–7181.

10. Kaidonis, X., Liaw, W.C., Roberts, A.D., Ly, M., Anson, D., and Byers, S. (2010). Gene silencing of EXTL2 and EXTL3 as a substrate deprivation therapy for heparan sulphate storing mucopolysaccharidoses. Eur. J. Hum. Genet. *18*, 194–199.
11. Takahashi, I., Noguchi, N., Nata, K., Yamada, S., Kaneiwa, T., Mizumoto, S., Ikeda, T., Sugihara, K., Asano, M., Yoshikawa, T., et al. (2009). Important role of heparan sulfate in postnatal islet growth and insulin secretion. Biochem. Biophys. Res. Commun. *383*, 113–118.
12. Bishop, J.R., Schuksz, M., and Esko, J.D. (2007). Heparan sulphate proteoglycans fine-tune mammalian physiology. Nature *446*, 1030–1037.
13. Rodgers, K.D., San Antonio, J.D., and Jacenko, O. (2008). Heparan sulfate proteoglycans: a GAGgle of skeletal-hematopoietic regulators. Dev. Dyn. *237*, 2622–2642.
14. Bruno, E., Luikart, S.D., Long, M.W., and Hoffman, R. (1995). Marrow-derived heparan sulfate proteoglycan mediates the adhesion of hematopoietic progenitor cells to cytokines. Exp. Hematol. *23*, 1212–1217.
15. McCormick, C., Duncan, G., Goutsos, K.T., and Tufaro, F. (2000). The putative tumor suppressors EXT1 and EXT2 form a stable complex that accumulates in the Golgi apparatus and catalyzes the synthesis of heparan sulfate. Proc. Natl. Acad. Sci. USA *97*, 668–673.
16. Farhan, S.M., Wang, J., Robinson, J.F., Prasad, A.N., Rupar, C.A., Siu, V.M., Hegele, R.A.; and FORGE Canada Consortium (2015). Old gene, new phenotype: mutations in heparan sulfate synthesis enzyme, EXT2 leads to seizure and developmental disorder, no exostoses. J. Med. Genet. *52*, 666–675.
17. Sobreira, N., Schiettecatte, F., Valle, D., and Hamosh, A. (2015). GeneMatcher: a matching tool for connecting investigators with an interest in the same gene. Hum. Mutat. *36*, 928–930.
18. Philippakis, A.A., Azzariti, D.R., Beltran, S., Brookes, A.J., Brownstein, C.A., Brudno, M., Brunner, H.G., Buske, O.J., Carey, K., Doll, C., et al. (2015). The Matchmaker Exchange: a platform for rare disease gene discovery. Hum. Mutat. *36*, 915–921.
19. Buske, O.J., Girdea, M., Dumitriu, S., Gallinger, B., Hartley, T., Trang, H., Misyura, A., Friedman, T., Beaulieu, C., Bone, W.P., et al. (2015). PhenomeCentral: a portal for phenotypic and genotypic matchmaking of patients with rare genetic diseases. Hum. Mutat. *36*, 931–940.
20. Becker, J., Semler, O., Gilissen, C., Li, Y., Bolz, H.J., Giunta, C., Bergmann, C., Rohrbach, M., Koerber, F., Zimmermann, K., et al. (2011). Exome sequencing identifies truncating mutations in human SERPINF1 in autosomal-recessive osteogenesis imperfecta. Am. J. Hum. Genet. *88*, 362–371.
21. Gilissen, C., Arts, H.H., Hoischen, A., Spruijt, L., Mans, D.A., Arts, P., van Lier, B., Steehouwer, M., van Reeuwijk, J., Kant, S.G., et al. (2010). Exome sequencing identifies WDR35 variants involved in Sensenbrenner syndrome. Am. J. Hum. Genet. *87*, 418–423.
22. Hoischen, A., van Bon, B.W., Gilissen, C., Arts, P., van Lier, B., Steehouwer, M., de Vries, P., de Reuver, R., Wieskamp, N., Mortier, G., et al. (2010). De novo mutations of SETBP1 cause Schinzel-Giedion syndrome. Nat. Genet. *42*, 483–485.
23. Hoischen, A., van Bon, B.W., Rodríguez-Santiago, B., Gilissen, C., Vissers, L.E., de Vries, P., Janssen, I., van Lier, B., Hastings, R., Smithson, S.F., et al. (2011). De novo nonsense mutations in ASXL1 cause Bohring-Opitz syndrome. Nat. Genet. *43*, 729–731.
24. Hempel, M., Cremer, K., Ockeloen, C.W., Lichtenbelt, K.D., Herkert, J.C., Denecke, J., Haack, T.B., Zink, A.M., Becker, J., Wohlleber, E., et al. (2015). De Novo Mutations in CHAMP1 Cause Intellectual Disability with Severe Speech Impairment. Am. J. Hum. Genet. *97*, 493–500.
25. Mendoza-Londono, R., Fahiminiya, S., Majewski, J., Tétreault, M., Nadaf, J., Kannu, P., Sochett, E., Howard, A., Stimec, J., Dupuis, L., et al.; Care4Rare Canada Consortium (2015). Recessive osteogenesis imperfecta caused by missense mutations in SPARC. Am. J. Hum. Genet. *96*, 979–985.
26. Srour, M., Hamdan, F.F., McKnight, D., Davis, E., Mandel, H., Schwartzentruber, J., Martin, B., Patry, L., Nassif, C., Dionne-Laporte, A., et al.; Care4Rare Canada Consortium (2015). Joubert Syndrome in French Canadians and Identification of Mutations in CEP104. Am. J. Hum. Genet. *97*, 744–753.
27. Le Quesne Stabej, P., Williams, H.J., James, C., Tekman, M., Stanescu, H.C., Kleta, R., Ocaka, L., Lescai, F., Storr, H.L., Bitner-Glindzicz, M., et al.; GOSgene (2016). STAG3 truncating variant as the cause of primary ovarian insufficiency. Eur. J. Hum. Genet. *24*, 135–138.
28. Li, H., Handsaker, B., Wysoker, A., Fennell, T., Ruan, J., Homer, N., Marth, G., Abecasis, G., Durbin, R.; and 1000 Genome Project Data Processing Subgroup (2009). The Sequence Alignment/Map format and SAMtools. Bioinformatics *25*, 2078–2079.
29. Krumm, N., Sudmant, P.H., Ko, A., O'Roak, B.J., Malig, M., Coe, B.P., Quinlan, A.R., Nickerson, D.A., Eichler, E.E.; and NHLBI Exome Sequencing Project (2012). Copy number variation detection and genotyping from exome sequence data. Genome Res. *22*, 1525–1532.
30. de Ligt, J., Boone, P.M., Pfundt, R., Vissers, L.E., Richmond, T., Geoghegan, J., O'Moore, K., de Leeuw, N., Shaw, C., Brunner, H.G., et al. (2013). Detection of clinically relevant copy number variants with whole-exome sequencing. Hum. Mutat. *34*, 1439–1448.
31. Shi, Y., and Majewski, J. (2013). FishingCNV: a graphical software package for detecting rare copy number variations in exome-sequencing data. Bioinformatics *29*, 1461–1462.
32. Fromer, M., Moran, J.L., Chambert, K., Banks, E., Bergen, S.E., Ruderfer, D.M., Handsaker, R.E., McCarroll, S.A., O'Donovan, M.C., Owen, M.J., et al. (2012). Discovery and statistical genotyping of copy-number variation from whole-exome sequencing depth. Am. J. Hum. Genet. *91*, 597–607.
33. Fromer, M., and Purcell, S.M. (2014). Using XHMM Software to Detect Copy Number Variation in Whole-Exome Sequencing Data. Curr. Protoc. Hum. Genet. *81*, 7.23.1–7.23.21.
34. Poultney, C.S., Goldberg, A.P., Drapeau, E., Kou, Y., Harony-Nicolas, H., Kajiwara, Y., De Rubeis, S., Durand, S., Stevens, C., Rehnström, K., et al. (2013). Identification of small exonic CNV from whole-exome sequence data and application to autism spectrum disorder. Am. J. Hum. Genet. *93*, 607–619.
35. Engels, H., Wohlleber, E., Zink, A., Hoyer, J., Ludwig, K.U., Brockschmidt, F.F., Wieczorek, D., Moog, U., Hellmann-Mersch, B., Weber, R.G., et al. (2009). A novel microdeletion syndrome involving 5q14.3-q15: clinical and molecular cytogenetic characterization of three patients. Eur. J. Hum. Genet. *17*, 1592–1599.
36. Abecasis, G.R., Auton, A., Brooks, L.D., DePristo, M.A., Durbin, R.M., Handsaker, R.E., Kang, H.M., Marth, G.T., McVean, G.A.; and 1000 Genomes Project Consortium (2012). An integrated map of genetic variation from 1,092 human genomes. Nature *491*, 56–65.

37. aan de Kerk, D.J., Jansen, M.H., ten Berge, I.J., van Leeuwen, E.M., and Kuijpers, T.W. (2013). Identification of B cell defects using age-defined reference ranges for in vivo and in vitro B cell differentiation. J. Immunol. *190*, 5012–5019.
38. Kuijpers, T.W., van Leeuwen, E.M., Barendregt, B.H., Klarenbeek, P., aan de Kerk, D.J., Baars, P.A., Jansen, M.H., de Vries, N., van Lier, R.A., and van der Burg, M. (2013). A reversion of an IL2RG mutation in combined immunodeficiency providing competitive advantage to the majority of CD8+ T cells. Haematologica *98*, 1030–1038.
39. Sanjana, N.E., Shalem, O., and Zhang, F. (2014). Improved vectors and genome-wide libraries for CRISPR screening. Nat. Methods *11*, 783–784.
40. Langereis, E.J., Wagemans, T., Kulik, W., Lefeber, D.J., van Lenthe, H., Oussoren, E., van der Ploeg, A.T., Ruijter, G.J., Wevers, R.A., Wijburg, F.A., and van Vlies, N. (2015). A Multiplex Assay for the Diagnosis of Mucopolysaccharidoses and Mucolipidoses. PLoS ONE *10*, e0138622.
41. Kingma, S.D., Wagemans, T., IJlst, L., Wijburg, F.A., and van Vlies, N. (2014). Genistein increases glycosaminoglycan levels in mucopolysaccharidosis type I cell models. J. Inherit. Metab. Dis. *37*, 813–821.
42. Lowry, O.H., Rosebrough, N.J., Farr, A.L., and Randall, R.J. (1951). Protein measurement with the Folin phenol reagent. J. Biol. Chem. *193*, 265–275.
43. Lawrence, R., Lu, H., Rosenberg, R.D., Esko, J.D., and Zhang, L. (2008). Disaccharide structure code for the easy representation of constituent oligosaccharides from glycosaminoglycans. Nat. Methods *5*, 291–292.
44. Pedersen, L.C., Dong, J., Taniguchi, F., Kitagawa, H., Krahn, J.M., Pedersen, L.G., Sugahara, K., and Negishi, M. (2003). Crystal structure of an alpha 1,4-N-acetylhexosaminyltransferase (EXTL2), a member of the exostosin gene family involved in heparan sulfate biosynthesis. J. Biol. Chem. *278*, 14420–14428.
45. Vissers, L.E., de Ligt, J., Gilissen, C., Janssen, I., Steehouwer, M., de Vries, P., van Lier, B., Arts, P., Wieskamp, N., del Rosario, M., et al. (2010). A de novo paradigm for mental retardation. Nat. Genet. *42*, 1109–1112.
46. Rothenberg, E.V., Ungerbäck, J., and Champhekar, A. (2016). Forging T-Lymphocyte Identity: Intersecting Networks of Transcriptional Control. Adv. Immunol. *129*, 109–174.
47. Lind, T., Tufaro, F., McCormick, C., Lindahl, U., and Lidholt, K. (1998). The putative tumor suppressors EXT1 and EXT2 are glycosyltransferases required for the biosynthesis of heparan sulfate. J. Biol. Chem. *273*, 26265–26268.
48. Lee, J.S., von der Hardt, S., Rusch, M.A., Stringer, S.E., Stickney, H.L., Talbot, W.S., Geisler, R., Nüsslein-Volhard, C., Selleck, S.B., Chien, C.B., and Roehl, H. (2004). Axon sorting in the optic tract requires HSPG synthesis by ext2 (dackel) and extl3 (boxer). Neuron *44*, 947–960.
49. Peterson, H.A. (1989). Multiple hereditary osteochondromata. Clin. Orthop. Relat. Res. (239), 222–230.
50. Forsberg, E., and Kjellén, L. (2001). Heparan sulfate: lessons from knockout mice. J. Clin. Invest. *108*, 175–180.